Approximate formulas and physical interpretations for horizontal acoustic modes in a shelf-slope front model

Brendan J. DeCourcy,[1] Ying-Tsong Lin,[2] and William L. Siegmann[1]

[1]*Department of Mathematical Sciences, Rensselaer Polytechnic Institute, Troy, New York 12180, USA*
[2]*Applied Ocean Physics and Engineering Department, Woods Hole Oceanographic Institution, Woods Hole, Massachusetts 02543, USA*
decoub@rpi.edu, ytlin@whoi.edu, siegmw@rpi.edu

Abstract: The structure and behavior of horizontal acoustic modes for a three-dimensional idealized model of a shelf-slope front are examined analytically. The Wentzel–Kramers–Brillouin–Jeffreys (WKBJ) method is used to obtain convenient simple expressions and to provide physical insight into the structure and behavior of horizontal modes as trapped, leaky, or transition types. Validity regions for WKBJ expressions in terms of slope and frontal parameters are found, and outside the regions the asymptotic formulas for large order and large argument Hankel functions are used. These combined approximations have very good accuracy as shown by comparisons with numerical solutions for modal shapes and horizontal wavenumbers.
© 2016 Acoustical Society of America
[DRD]

1. Introduction

Recent research in shallow water ocean acoustic propagation examines the influences of three dimensional (3-D) ocean feature models, such as the idealized coastal front model of Lin and Lynch.[1] The motivation for this paper is to demonstrate how ocean environment variability that is characterized by feature model parameters can affect acoustic quantities. One approach is to use numerical computations with different parameter values, but the relevant parameter ranges can be large. Another approach is to find accurate approximate formulas which determine how acoustic quantities depend on model parameters, with Ref. 2 containing a classic illustration for a 2-D model. Such formulas are useful for sensitivity investigations and for revealing physical insights into feature influences that are hidden in computations. The objective of this paper is to illustrate, for the feature model in Ref. 1, an approximation approach that lays the foundation for determining how acoustic quantities of interest depend on feature parameters.

The 3-D coastal front model[1] is sketched in Fig. 1(a), with cylindrical coordinates (r, θ, y), where the y-axis is the shoreline and the curved front is $r = r_I$. Other model parameters are an assumed constant density ρ, constant sound speeds c_1 (inshore), and c_2 (offshore) on either side of the front, and a constant bottom slope angle α. The shallow ocean lies inside the wedge with a pressure release surface and a hard reflecting bottom.

The approximation approach for normal mode quantities emphasizes the Wentzel–Kramers–Brillouin–Jeffreys (WKBJ) method. This technique has been widely used in ocean acoustics, as in approximating mode functions in 3-D wedge geometry,[3] and acoustic fields near caustics.[4] Asymptotic approximations are also used to simplify expressions containing large order and large argument Hankel/Bessel functions.[5] The results illustrate the accuracy of approximations for both horizontal wavenumbers and mode shapes. This paper is a step toward the eventual goal of using such approximations to find convenient and accurate formulas for determining the sensitivity of acoustic quantities to parameter variations, both in this coastal slope front model and others such as internal waves[6] and seamounts.[7]

2. Review of previous analytical solution

Throughout this section the approach in Ref. 1 is followed. The acoustic pressure in the wedge resulting from an inshore point source of one frequency f at location $(r_0, \theta_0, 0)$ is expressed by the Fourier integral
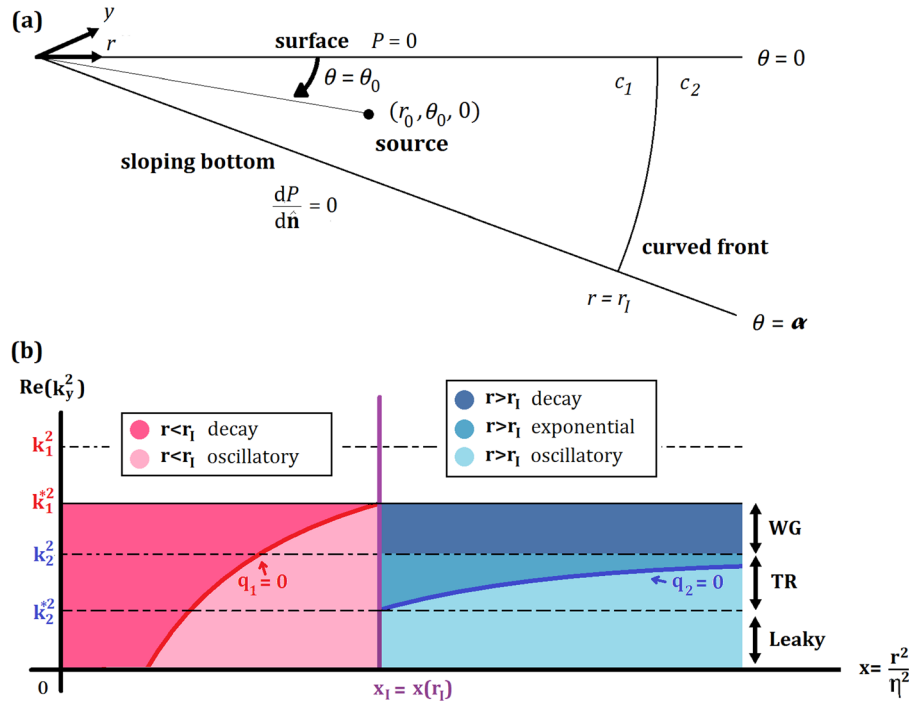
Fig. 1. (Color online) (a) Geometry of shelf-slope model and cylindrical coordinate system (r, θ, y). Reference parameter values are $r_I = 4000$ m, $\alpha = 3°$, $f = 25$ Hz, $c_1 = 1500$ ms^{-1}, and $c_2 = 1520$ ms^{-1}. Based on figure from Ref. 1. (b) Sketch of radial mode types and behavior on both sides of the front, showing $\mathrm{Re}(k_y^2)$ versus scaled range $x = (r/\eta)^2$ for angular wavenumber η. For $n = 1$ (shown), mode types are trapped [or whispering gallery (WG)] for $k_1^* > k_y > k_2$; transition (TR) for $k_2 > k_y > k_2^*$; and leaky for $k_2^* > k_y > 0$. This example is appropriate for the reference parameter values. For cases $n \geq 2$, k_2 is greater than k_1^*, so no WG region occurs.

$$P(r, \theta, y) = \frac{1}{2\pi} \int_{-\infty}^{\infty} G(r, \theta, k_y) e^{ik_y y} dk_y \qquad (1)$$

with horizontal (along-front) wavenumber k_y and Green's function G. An analytical expression for the solution P for large y is found by a method used in the problem with no front.[8] The function G is obtained using separation of variables and the endpoint method. The integral in Eq. (1) is approximated in the far field by using the Pekeris branch cut in the k_y-plane, neglecting branch line integrals, and evaluating the residues at poles. The result corresponds to Eq. (9) of Ref. 1:

$$P(r, \theta, y) \approx \sum_n \sum_m Q_{nm} \Phi_n(\theta_0) \Psi_{nm}(r_0, k_{y,nm}) \Phi_n(\theta) \Psi_{nm}(r, k_{y,nm}) e^{ik_{y,nm}y}, \qquad (2)$$

where Φ_n and Ψ_{nm} are angular and radial modes, n and m are the angular and radial mode numbers, and Q_{nm} is a normalization constant for Ψ_{nm}. The boundary conditions of a pressure release surface $[\Phi_n(0) = 0]$ and a hard reflecting bottom $[\Phi'_n(\alpha) = 0]$ produce $\Phi_n(\theta) = \sqrt{2/\alpha\pi} \sin(\eta_n \theta)$, with the angular wavenumber $\eta_n = (\pi/\alpha)(n - 1/2)$.

The radial modes Ψ_{nm} are solutions to

$$\frac{1}{r}\frac{d}{dr}\left[r\frac{d\Psi_{nm}(r, k_{y,nm})}{dr}\right] + \left(k_j^2 - k_{y,nm}^2 - \frac{\eta_n^2}{r^2}\right)\Psi_{nm}(r, k_{y,nm}) = 0, \qquad (3)$$

where k_j is the medium wavenumber and j denotes the inshore ($j = 1$, $r < r_I$) or off-shore ($j = 2$, $r > r_I$) region. The solution Ψ_{nm} satisfies the boundary and interface conditions of finiteness at $r = 0$, a Sommerfield radiation condition as $r \to \infty$, and continuity with continuous derivative at $r = r_I$:

$$\Psi_{nm}(r) = \begin{cases} J_{\eta_n}(k_{r1,nm}r), & r_I \geq r \geq 0, \\ \left(J_{\eta_n}(k_{r1,nm}r_I)/H_{\eta_n}^{(1)}(k_{r2,nm}r_I)\right)H_{\eta_n}^{(1)}(k_{r2,nm}r), & r \geq r_I, \end{cases} \qquad (4)$$

where $k_{rj,nm} = \sqrt{k_j^2 - k_{y,nm}^2}$. The dispersion relation for k_y is a complicated formula involving Hankel functions [Ref. 1, Eq. (5)], an equivalent form of which is

$$k_{r1,nm} \frac{J'_{\eta_n}(k_{r1,nm}r_I)}{J_{\eta_n}(k_{r1,nm}r_I)} = k_{r2,nm} \frac{H^{(1)}_{\eta_n}{}'(k_{r2,nm}r_I)}{H^{(1)}_{\eta_n}(k_{r2,nm}r_I)}. \tag{5}$$

The dependence of the eigenvalues $k_{y,nm}$ on model parameters from Eq. (5) is opaque, motivating the use of approximation methods.

3. Approximations of the normal modes and dispersion relation

Our eventual goal is to determine how model parameter variations influence acoustic quantities. An intermediate step after this paper is to find convenient formulas expressing the parameter variations of the wavenumbers $k_{y,nm}$ (or the modal phase speeds $2\pi f/k_{y,nm}$). To obtain such formulas from a simplified dispersion relation, approximate formulas are first found for radial mode functions Ψ (mode numbers n and m are subsequently dropped on Ψ, k_{rj}, k_y, and η). Equation (3) is transformed using $B(r) = r^{1/2}\Psi(r)$, yielding

$$(\eta^2 - 1/4)^{-1}B'' - q_j(r)B = 0, \quad q_j(r; k_y) = r^{-2} - (\eta^2 - 1/4)^{-1}k_{rj}^2. \tag{6}$$

The first approximation will be to replace $(\eta^2 - 1/4)^{-1}$ with η^{-2}. This is a good approximation, because $\eta^2 \geq 900 \gg 1/4$ for the reference parameters in Fig. 1(a).

Simple approximations for solutions to Eq. (6) can be found over regions where the function q_j does not change sign, having either exponential ($q_j > 0$) or oscillatory ($q_j < 0$) behavior. Where q_j changes sign a turning point in r occurs at $r = 1/\eta^{-2}k_{rj} \equiv r_{tj}$, and separates exponential from oscillatory modal behavior. The possible behaviors of $B(r)$ are illustrated in Fig. 1(b) for representative parameter values. The horizontal axis represents a scaled distance $x = (r/\eta)^2$ from the apex of the wedge, with the vertical line at $x = x_I$ denoting the front location. The vertical axis represents the real part of k_y^2. Although k_y can be complex, the imaginary part is small compared with the real part as will be seen later. The two solid curves $q_j = 0$ in Fig. 1(b) show locations of turning points inshore (left) and offshore (right) of the front.

Inshore, all radial modes have the same characteristics of exponential decay closer to shore and oscillations closer to the front as suggested by Fig. 1(b). The modes that decay exponentially offshore are trapped and are whispering gallery (WG) modes, which have no decay in the along-shore y direction. Modes that are oscillatory everywhere offshore are leaky with small but non-negligible decay in y. Some modes possess both exponential and oscillatory behavior offshore and are called transition (TR) modes, which require more care to approximate. Because trapped acoustic energy and oscillatory behavior are required for modes in some inshore region, q_1 must be negative there. Therefore, the largest value of k_y for any such mode is k_1^* where $q_1(r_I; k_1^*) = 0$, which imposes an upper bound on k_y: $k_y < \sqrt{k_1^2 - \eta^2/r_I^2} \equiv k_1^*$.

Inshore of the front ($r < r_I$) all modes are approximated by the WKBJ solution to Eq. (6) with a turning point[9] at $r_{t1} < r_I$:

$$\Psi_{inshore}(r) \sim \begin{cases} (2\pi\eta)^{-1/2}[1 - (k_{r1}r/\eta)^2]^{-1/4}e^{-\eta\sigma_1(r)}, & r_{t1} \geq r \geq 0, \\ (2\pi\eta)^{-1/2}[(k_{r1}r/\eta)^2 - 1]^{-1/4}\sin(\eta\kappa_1(r) + \pi/4), & r_I \geq r_{t1}. \end{cases} \tag{7}$$

In Eq. (7) the functions σ_1 and κ_1 are defined by

$$\sigma_j(r) = \log\left(\frac{1 + \sqrt{1 - \beta_j^2 r^2}}{\alpha_j r}\right) - \sqrt{1 - \beta_j^2 r^2}, \quad \kappa_j(r) = \sqrt{\beta_j^2 - 1} - \cos^{-1}\left(\frac{1}{\beta_j r}\right), \tag{8}$$

and constants $\beta_j = k_{rj}/\eta$, for $j = 1$, and the same definitions apply for $j = 2$.

Offshore of the front, there are three cases: (A) $q_2 > 0$ for all $r > r_I$ (leaky modes), (B) $q_2 < 0$ for all $r > r_I$ (trapped), or (C) $q_2 = 0$ for some $r > r_I$ (transition). In cases (A) and (B) for which no offshore turning point exists, the WKBJ method is used.[9] The radiation condition for large r and mode continuity with Eq. (7) at the front $r = r_I$ is imposed, leading to the radial mode approximations

$$\Psi_{trapped}(r) \sim \left[\left(\frac{\eta^2 - k_{r2}^2 r_I^2}{k_{r1}^2 r_I^2 - \eta^2}\right)^{1/4} \frac{\sin(\eta\kappa_1(r_I) + \pi/4)}{e^{\eta\sigma_2(r_I)}}\right] \sqrt{\frac{2}{\pi\eta}}\left(1 - \frac{k_{r2}^2}{\eta^2}r^2\right)^{-1/4} e^{\eta\sigma_2(r)}, \tag{9}$$

$$\Psi_{leaky}(r) \sim \left[\left(\frac{k_{r2}^2 r_I^2 - \eta^2}{k_{r1}^2 r_I^2 - \eta^2} \right)^{1/4} \frac{\sin(\eta\kappa_1(r_I) + \pi/4)}{e^{i\eta\kappa_2(r_I)}} \right] \sqrt{\frac{2}{\pi\eta}} \left(\frac{k_{r2}^2}{\eta^2} r^2 - 1 \right)^{-1/4} e^{i\eta\kappa_2(r)}. \quad (10)$$

The WKBJ solutions are valid for[9]

$$k_{rj}|r - r_{tj}| \gg \eta^{1/3}. \quad (11)$$

In case (C) there is a turning point that requires $k_2^* < k_y < k_2$ where $q_2(r_I; k_2^*) = 0$, and $k_2^* = \sqrt{k_2^2 - \eta^2/r_I^2}$ is a lower bound for k_y. Because Eq. (11) generally does not hold close to the front location, asymptotic approximations of Hankel functions are used instead of the WKBJ solutions. Because both the order and argument of the Hankel and Bessel functions in Eq. (4) are large, the following TR mode expression can be derived by first applying large order, large argument Bessel and Hankel function approximations, and then using a large order Airy function approximation,[10]

$$\Psi_{transition}(r) \sim \begin{cases} \rho_t (2/\pi\eta)^{1/2}[1 - (k_{r2}r/\eta)^2]^{-1/4} \sin(\pi/4 - i\eta\sigma_2(r)), & r_{t2} \geq r \geq r_I, \\ \rho_t (2\pi\eta)^{-1/2}[(k_{r2}r/\eta)^2 - 1]^{-1/4} e^{-i\pi/4} e^{i\eta\kappa_2(r)}, & r \geq r_{t2}, \end{cases} \quad (12)$$

where

$$\rho_t = \left(\frac{\eta^2 - k_{r2}^2 r_I^2}{k_{r1}^2 r_I^2 - \eta^2} \right)^{1/4} \frac{\sin(\eta\kappa_1(r_I) + \pi/4)}{\sin(\pi/4 - i\eta\sigma_2(r_I))}. \quad (13)$$

To obtain approximations to the dispersion relation for each mode type, the interface condition of smoothness at $r = r_I$ is applied to the approximations in Eqs. (7)–(10) and Eqs. (12), (13). After lengthy algebra, identical dispersion relations arise for the trapped and leaky modes, along with another relation for transition modes,

$$\text{Trapped and leaky modes:} \quad \tan\left(\eta\kappa_1(r_I) - \frac{\pi}{4} \right) = -i \frac{\sqrt{k_{r2}^2 r_I^2 - \eta^2}}{\sqrt{k_{r1}^2 r_I^2 - \eta^2}} + O(\eta^{-2}), \quad (14)$$

$$\text{Transition modes:} \quad \tan\left(\eta\kappa_1(r_I) - \frac{\pi}{4} \right) = -\frac{\sqrt{k_{r2}^2 r_I^2 - \eta^2}}{\sqrt{k_{r1}^2 r_I^2 - \eta^2}} \cot\left(\frac{\pi}{4} - i\eta\sigma_2(r_I) \right) + O(\eta^{-2}). \quad (15)$$

4. Accuracy of approximations

To examine the accuracy of results in Sec. 3, wavenumber solutions to the approximate dispersion relations given by Eqs. (14) and (15) are compared to high-accuracy values of k_y from Eq. (5). In addition, radial mode approximations Eqs. (7)–(10) and Eqs. (12), (13) are compared to high-accuracy evaluations of the exact solution Eq. (4).

In Fig. 2(a) high-accuracy wavenumbers for the parameters used in Fig. 1 are plotted for angular modes n = 1 (circles), 2 (triangles), and 3 (squares) in the complex k_y–plane, along with their corresponding approximations (crosses). The vertical dashed lines represent $\text{Re}(k_y) = k_2^*$ for $n = 1$, 2, and 3, and highlight the turning point in k_y that separates the leaky modes on the left from the TR modes on the right. The solid vertical line represents $\text{Re}(k_y) = k_2$, which separates WG modes on the right from TR and leaky modes on the left. For $n = 1$ the agreement is excellent for the nine WG modes, two TR modes, and all the leaky modes shown. For $n = 2$ there are no WG modes, and the agreement is excellent for all but one of the leaky modes shown and one of the three TR modes. For the two modes for which the agreement is less than excellent, the real parts are still very close, and the much smaller imaginary parts agree to about two significant digits. These two modes are close to the dashed vertical line which represents $\text{Re}(k_y) = k_2^*$, which is the spectral location of a turning point. The situation is similar for $n = 3$, with three leaky modes shown and two TR modes. One of the latter occurs almost exactly at the turning point, so its imaginary part has a significant relative error. Thus, apart from wavenumbers that are very close to k_2^*, the approximations are very accurate and should be adequate for examining parameter dependence.

Another accuracy test is to compare exact and approximate interference wavelengths for adjacent modes, $\Lambda_{m,m+1} = 2\pi/\text{Re}(k_{y,m} - k_{y,m+1})$. Figure 2(b) shows $\Lambda_{m,m+1}$ versus m for $n = 1$, and illustrates the close agreement between the exact solution (circles) and the approximation (crosses). Figure 2(c) shows the relative percentage
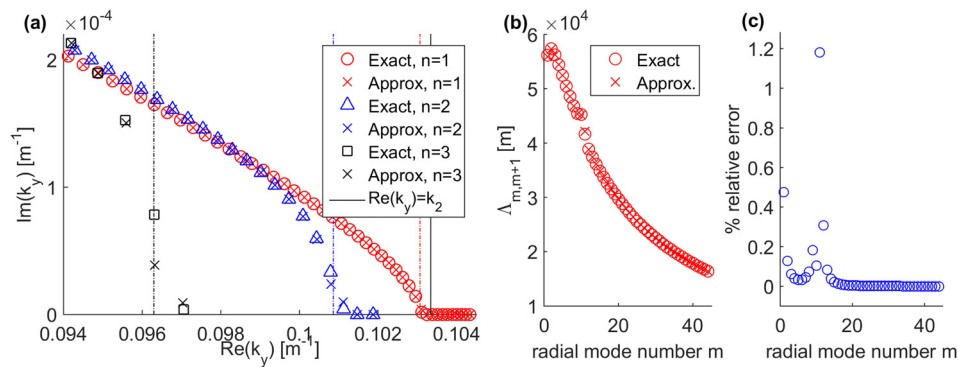
Fig. 2. (Color online) Parameter values as for Fig. 1. (a) Comparison between approximate (crosses) and high-accuracy (symbols) real and imaginary parts of wavenumbers k_y, for $n = 1$ (circles), 2 (triangles), and 3 (squares). Three dashed lines for $n = 1$, 2, and 3 represent $\mathrm{Re}(k_y) = k_2^*$, the maximum real k_y value for leaky modes. These turning points separate leaky modes (left of line) from transition modes (right of line), with the right-most line corresponding to $n = 1$ and left-most to $n = 3$. (b) Interference wavelength $\Lambda_{m,m+1}$ for adjacent modes and $n = 1$, showing exact values (circles) and approximations (crosses). (c) Relative percentage error of the interference wavelength approximations in (b).

error of the approximation which is very small and less than 1% excepting one pair of modes (the last transition and first leaky).

Comparisons are shown in Fig. 3 for three radial modes for $n = 1$, with the evaluation of analytic solutions shown as thick lines and approximate solutions shown as thin. All expected properties are visible in the real parts: the WG mode [$m = 4$, Fig. 3(a)] is trapped inshore of the front; the energy-leaking TR mode [$m = 11$, Fig. 3(c)] changes from exponential to oscillatory offshore; oscillations of the leaky mode [$m = 15$, Fig. 3(e)] become slower across the front from inshore to offshore. Agreement between thick and thin curves is excellent except in small regions demarcated by circles around inshore and offshore turning points (shown as crosses). The circles are defined by equality in Eq. (11), to specify where the asymptotic approximations are used. Analogous remarks apply for the corresponding imaginary parts: the WG mode [$m = 4$, Fig. 3(b)] has no imaginary part; the TR mode [$m = 11$, Fig. 3(d)] shows hybrid behavior; and the leaky mode [$m = 15$, Fig. 3(f)] has a substantial imaginary part. The imaginary parts of the approximations, like the real parts, have essentially no disagreement with the exact solutions except near the turning points in r.

In summary, the approximate modal solutions are excellent matches to the exact analytic solutions, except near turning points in range and for modes associated with wavenumbers k_y that are very close to curves separating transition and leaky modes.

5. Conclusion

The modal solutions of an idealized model of an oceanic front over a sloping bottom are analyzed using the WKBJ method and large order, large argument asymptotic
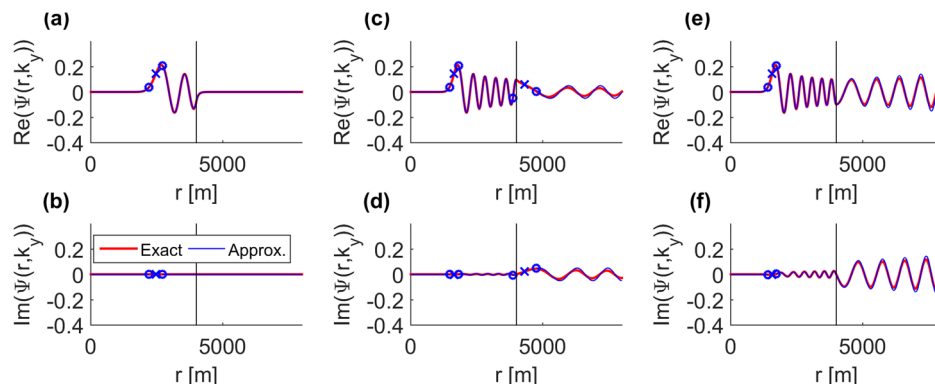

Fig. 3. (Color online) Comparison between approximate (thin curves) and exact (thick curves) real and imaginary parts of radial mode functions versus range r for parameter values in Fig. 1. The vertical line at $r_I = 4000$ m represents the front. Real parts for (a) WG mode $m = 4$, (c) TR mode $m = 11$, and (e) leaky mode $m = 15$, and corresponding imaginary parts in (b), (d), and (f). Approximate mode shapes are seen to be excellent approximations to exact shapes, except in narrow range interval bounded by two circles and containing a turning point (cross) where approximation is invalid.

approximations for Hankel functions. The dispersion relation that specifies horizontal modal wavenumbers k_y is also approximated, from which accurate k_y values can be found. It is shown that the spectrum of real k_y values is divided into three regions associated with distinct mode types: trapped or whispering gallery, leaky, and transition, and that the associated approximate mode functions provide insights into their different physical behaviors. The approximate dispersion relation formula is the same for both trapped and leaky modes, while the result for transition modes is somewhat more complicated. For both trapped and leaky modes, the radial mode shapes and the horizontal wavenumbers agree very well with results from high accuracy numerical solutions. These approximations will be used in future work to derive convenient and accurate approximations for parameter dependence of modal wavenumbers, modal phase speed, and other acoustic quantities.

Acknowledgments

References and links

[1] Y.-T. Lin and J. F. Lynch, "Analytical study of the horizontal ducting of sound by an oceanic front over a slope," J. Acoust. Soc. Am. **131**, EL1–EL7 (2012).

[2] A. D. Pierce, "Parametric solution of the dispersion relation for guided sound propagation in shallow water," J. Acoust. Soc. Am. **39**, 1139–1141 (1966).

[3] P. C. Mignerey, "Environmentally adaptive wedge modes," J. Acoust. Soc. Am. **107**, 1943–1952 (2000).

[4] C. T. Tindle, "Wavefronts and waveforms in deep-water sound propagation," J. Acoust. Soc. Am. **112**, 464–475 (2002).

[5] J. Fong, M. J. S. Lowe, D. Gridin, and R. V. Craster, "Fast techniques for calculating dispersion relations of circumferential waves in annular structures," Rev. Quant. Nondestruct. Eval. **22**, 213–220 (2003).

[6] Y.-T. Lin, K. G. McMahon, J. F. Lynch, and W. L. Siegmann, "Horizontal ducting of sound by curved nonlinear internal gravity waves in the continental shelf areas," J. Acoust. Soc. Am. **133**, 37–49 (2013).

[7] W. Luo and H. Schmidt, "Three-dimensional propagation and scattering around a conical seamount," J. Acoust. Soc. Am. **125**, 52–65 (2009).

[8] G. V. Frisk, *Ocean and Seabed Acoustics* (Prentice-Hall, Englewood Cliffs, NJ, 1994), pp. 275–280.

[9] M. H. Holmes, *Introduction to Perturbation Methods* (Springer, New York, 2013), pp. 236–243.

[10] M. Abramowitz and I. A. Stegun, *Handbook of Mathematical Functions, Vol. 55 of Applied Mathematics Series* (National Bureau of Standards, Washington, DC, 1964), pp. 368, 448, 449.